Facile Growth of 1-D Nanowire-Based WO_3 Thin Films with Enhanced Photoelectrochemical Performance

Jin-Rui Ding and Kyo-Seon Kim
Dept. of Chemical Engineering, Kangwon National University, Chuncheon, Kangwon-Do 200-701, Korea

DOI 10.1002/aic.15105
Published online November 28, 2015 in Wiley Online Library (wileyonlinelibrary.com)

A flame reactor embedded with a constant tungsten wire feeding system to prepare one-dimensional (1-D) nanostructured tungsten oxide thin film for photoelectrochemical (PEC) water splitting was developed. Photoactive vertically-aligned nanowire-based WO_3 thin films could be obtained with a controlled thickness via a flame vapor deposition process followed by air-annealing. The PEC performances of WO_3 photoelectrodes for different thin film thicknesses were examined. The optimum thickness of WO_3 thin film was found to be about 7.2 μm for PEC water splitting based on incident photon-to-current efficiency plots and I–V curves. The WO_3 prepared with optimum thickness showed better PEC performance than those of recently reported nanostructured WO_3 photoanodes. © 2015 American Institute of Chemical Engineers *AIChE J*, 62: 421–428, 2016

Keywords: nanowire, WO_3 thin films, optimum thickness, flame vapor deposition process, photoelctrochemical water splitting

Introduction

Photoelectrochemical (PEC) water splitting using semiconductor photoelectrodes is one of the most promising and environmentally friendly methods of producing hydrogen from water by utilizing renewable solar energy. Enormous efforts are being devoted to finding adequate semiconductor materials for photoelectrodes. The ideal semiconductor materials have to satisfy several requirements as follows: suitable band gap energy levels both for visible light absorption and for favorable energetic alignment to enable water oxidation and reduction, good electron transport properties, chemical and electrochemical stability in an aqueous solution under illumination, and low over-potentials for the electrode reactions as well as being relatively inexpensive.[1–4] Tungsten oxide (WO_3) is one of the most attractive semiconductor materials for PEC water splitting due to its energetically favorable valence band position for water oxidation, suitable band gap energy ($\sim$2.6 eV) for harvesting considerable light within the solar spectrum ($\sim$12%),[5] and appreciable photostability in water (<pH 4).[6]

The morphology of WO_3 thin films has been considered one of the important efficiency-limiting aspects of increasing the utility for water splitting. one-dimensional (1-D) nanostructures, such as nanowires,[7,8] nanorods,[9,10] and nanotubes,[7] which are normally oriented to the substrate, are favorable for PEC water spitting. This is due to the fact that 1-D structures orthogonalize the directions of electron migration along the long axis to charge the collector and hole transport across the short radius to the semiconductor/electrolyte interface. Besides, the long-range orientation allows inward light scattering leading to more efficient light absorption. The ideal 1-D nanostructures should be long enough for light absorption and, meanwhile, not too large for efficient charge transport. It was reported that WO_3 has the hole diffusion length at approximately 150 nm.[11] 1-D nanostructures with a diameter less than 300 nm would be desirable to diffuse holes efficiently to the WO_3/electrolyte interface. A dense WO_3 film with a thickness of approximately 6 μm is needed to absorb all the solar photons with energies above the bandgap of WO_3.[11] Thus, to maximize both light absorption and charge collection, 1-D nanostructured WO_3 thin film with thicknesses up to 6 μm is preferable. This requires a robust technique for rapid and continuous growth of highly oriented 1-D WO_3 thin films. Chakrapani's group[12] has synthesized WO_3 nanowire arrays by a chemical vapor deposition (CVD) process involving a flow of oxygen over a hot tungsten filament in a vacuum system. Su et al.[8] prepared WO_3 nanowires by performing a solvothermal method using tungstic acid as a precursor, in which a seed layer was deposited on conductive glass substrate by spin coating before the solvothermal growth. Because this technique is self-limiting on a finite supply of reactants and has a low operating temperature, it results in not only a slow growth rate and limited thickness but also low crystallinity and low purity of products[13] as well as the difficulty to scale up.[14] Zheng's group[7,15] has pioneered the growth of nanowire-based tungsten oxide thin film on conductive (FTO coated) glass by flame synthesis, where tungsten wire mesh was used as a precursor source located in the flame. It is quite difficult to keep vapor concentration constant over time and to get the desirable thickness of the thin film.

In our study, we developed a facile and economical flame vapor deposition (FVD) process, in which a solid wire feeding system was first incorporated into the flame reactor realizing a constant tungsten feed rate, which can guarantee the constant

Additional Supporting Information may be found in the online version of this article.

Correspondence concerning this article should be addressed to K.-S. Kim at kkyoseon@kangwon.ac.kr.

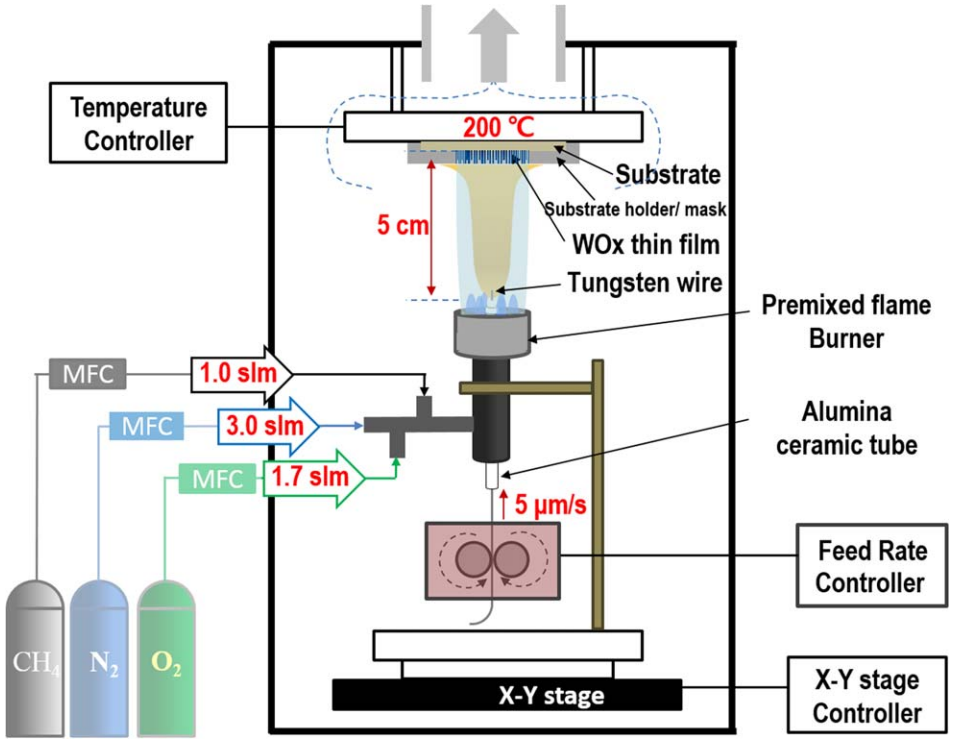

Figure 1. The schematic of experimental setup of FVD process for nanowire-based tungsten oxide thin films growth.

[Color figure can be viewed in the online issue, which is available at wileyonlinelibrary.com.]

vapor concentration in an FVD system. Vertically-aligned nanowire-based thin films of substoichiometric tungsten oxide were prepared with a controllable thickness, which could be converted to photoactive monoclinic WO_3 by postannealing. The thin film growth rate was fast enough to reach up to a few hundred nanometers per minute. The WO_3 nanostructured thin film prepared in this study showed better performances of PEC water splitting than those recently reported in the literature.

Experimental

Thin film preparation and characterization

The experimental set up for the FVD process is shown schematically in Figure 1. It mainly consists of three parts: Part 1, the premixed flame burner, where the various gases such as CH_4, O_2, and N_2 were introduced with flow rates precisely controlled and were well mixed in the chamber prior to the nozzles of the premixed flame burner; Part 2, the constant feeding system, where the feed rate controller supplies the tungsten wire (precursor, 0.025 cm in diameter, $\geq$99.9% purity, Sigma-Aldrich) with a constant feed rate from the bottom of a temperature-resistant alumina ceramic tube, which is embedded in the central nozzle of the premixed burner; Part 3, the substrate temperature controlling system, where the FTO-coated glass substrate (2 mm in thickness and 1.5 $\times$ 1.5 cm^2 in area, Sigma-Aldrich) was held by a substrate holder with an exposed area of 1 $\times$ 1 cm^2 and was attached on a temperature controlled plate. A small amount of silver thermal paste (Arctic Silver, Visalia, CA) was adhered to the backside of the substrate to keep intimate thermal contact between the substrate and temperature controlled plate. The tungsten wire evaporated and was partially oxidized in the high temperature atmosphere of the methane-oxygen fuel rich flame generating a vapor species which included a mixture of WO_x ($x < 3$) and/or $WC_xO_yH_z$, These vapor species are designated WO_x in the following context. These vapors were transported downstream by convection and diffusion, and subsequently, were condensed onto FTO-coated glass substrate to form substoichiometric WO_x thin film. Nanowire-based tungsten oxide thin films were obtained in the experimental conditions as follows: tungsten wire feed rate: 5 μm/s, deposition height: 5 cm, substrate temperature: 200°C, fuel-rich flame (1.0 slm (liter per minute at standard temperature and pressure) of CH_4 and molar ratios of CH_4:O_2:N_2 = 1:1.7:3). The calculated adiabatic flame temperature of this premix flame is about 2849°C. Thin films were prepared for various deposition times (t_D: 10–40 min) to obtain thin film with different thicknesses. The as-grown thin films were annealed in air at 450°C for 2 h before being assembled into the photoelectrode for the PEC test.

The morphology, thickness, and crystal structure of the tungsten oxide thin films were characterized by scanning electron microscopy (UHR-SEM, Hitachi S-4800) and X-ray diffraction (HRXRD, X'Pert PRO MPD), respectively.

Photoelectrochemical measurements

The WO_x thin films grown on the FTO substrate were fabricated as working electrodes (WE) for PEC measurement. A copper wire was bonded through high-purity silver conducting paint onto a bare part of the FTO substrate. The bare part of the substrate edges and the metal contact regions were sealed with insulating epoxy resin to prevent photocurrent leakage. The WE was masked to use only an area of 0.25 cm^2 in the central part (reasonably uniform deposition of thin film could be ensured within this area) for light illumination. PEC measurements were performed using a three-electrode electrochemical custom-built photocell with an embedded quartz window,

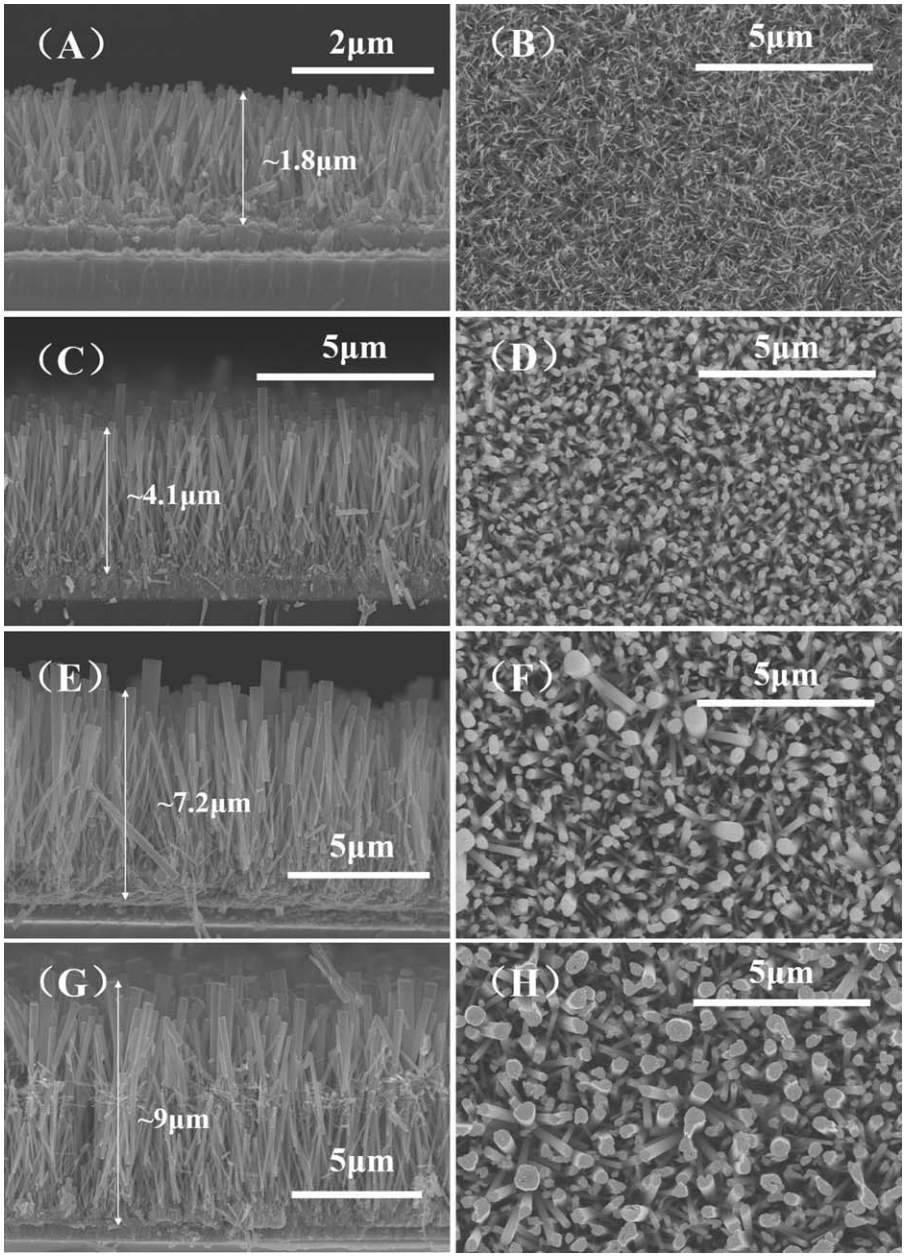

Figure 2. SEM images of as-grown tungsten oxide thin films prepared for various deposition time.

(A, B) 10 min, (C, D) 20 min, (E, F) 30 min. (G, H) 40 min.

equipped with a saturated calomel electrode (SCE) as reference electrode and a platinum mesh as counter electrode (CE). The photocell was filled with an aqueous solution of 0.5 M H_2SO_4 as an electrolyte. The distance between WE and CE was kept at 1 cm. A 300 W xenon lamp coupled with a monochromator (Mmac 200, Spectro, Korea) was used to select the wavelength of light for the incident photon-to-current efficiency (IPCE) measurement. Linear sweep voltammetry was performed under illumination of simulated sunlight obtained from a 300 W xenon lamp coupled with an AM1.5 G filter. The scan rate for all linear sweep voltammetry was 10 m Vs^{-1}. The light intensity of 100 mW cm^{-2} was calibrated by an optical power meter (PM100D, Thorlabs) with Sensor (S140C). The current was recorded by a Potentiostat (Versastat 3, Princeton Applied Research). All PEC measurements were performed in an argon atmosphere. The IPCE values were calculated using the following expression[16]: IPCE $(\%) = 1240 \times \frac{J\left(A\ \mathrm{cm}^{-2}\right)}{\lambda(\mathrm{nm}) \times P(W\ \mathrm{cm}^{-2})}) \times 100$, where J and P are the photocurrent density and light irradiance, respectively, for a certain wavelength region of incident light and λ corresponds to the average wavelength.

Results and Discussion

Thin film preparation and characterization

The experimental conditions mentioned in the experimental section were found to be favorable for 1-D nanowire-based thin film growth and were maintained for all thin film deposition experiments in this study. WO_x thin films with controlled thicknesses were prepared for different deposition times from 10 to 40 min. The typical SEM images of as-grown thin films are shown in Figure 2(A–H). All thin films showed the morphologies of vertically aligned nanowire-based structures.

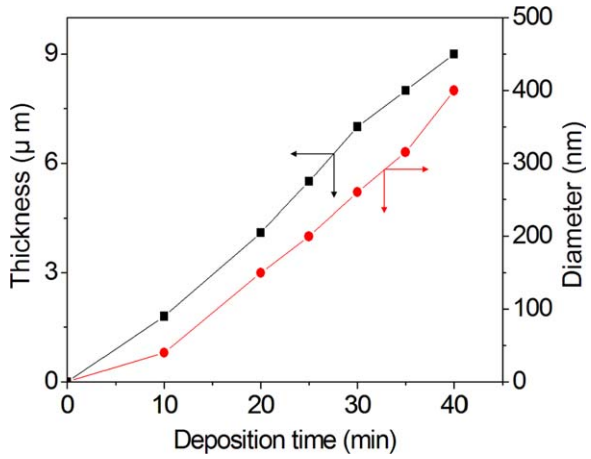

Figure 3. The curves of thin films thickness (A) and nanowire diameter (B) with respect to deposition time.

[Color figure can be viewed in the online issue, which is available at wileyonlinelibrary.com.]

When the thin film was prepared for 10 min as shown in Figures 2A, B, the thickness was approximately 1.8 μm and the diameter of the nanowires ranged from 30 to 50 nm. After 30 min deposition, the thickness increased to about 7.2 μm and the diameter of nanowires also increased. As thin film deposition was performed for 40 min, thin film thicknesses with nanowire-based structures reached up to 9 μm with an average diameter of about 400 nm. The thin film thickness and diameter of the individual structures grew larger with the increase of deposition time, as illustrated in Figure 3. In the meanwhile, the areal number density of nanowire-based structures decreases with deposition time. Based on our observation of these structural changes at various growth stages, the feasible growth mechanisms for these vertically aligned nanowire-based structures are illustrated in Figure 4. At the beginning of deposition, the generated WO_x vapors and small particles formed in the downstream could selectively be deposited on the surface of the FTO coated glass substrate to generate many nuclei for thin film growth, where the FTO layer has 145 nm in roughness and 650 nm in thickness (Supporting Information Figure S1). It was reported that substoichiometric WO_x formed under fuel-rich conditions has an intrinsically anisotropic growth property, leading to 1-D growth[7]. An et al.[17] pointed out that when a vapor and particles are coexisting in the downstream deposition region, 1-D nanostructures could be easily formed. And for vapor existing only, it tends to have an isotropic growth property and consequently smooth thin film could be formed. It is suggested that incoming vapors with small particles can be diffused and condensed much easier onto the top region of nanowires rather than penetrating deep into the bottom space between nanowires for shorter traveling distances. Besides, the high setting substrate temperature also has a great impact on 1-D nanostructure growth due to a sintering process.[18] Gradually, the growth in the axial direction becomes dominant compared to the lateral direction and the nanowire structures are formed. Because of the roughness of the original FTO surface, some individual nanowires happen to become taller than others and they can become dominant in growth, because the incoming vapors can be more selectively and easily diffused and condensed onto the taller ones by reduced traveling distances compared to the shorter ones. For the fixed flux of WO_x vapors, the taller ones receive more WO_x vapors than the shorter ones and they become taller and larger in diameter than the shorter ones over time, which is demonstrated in Figure 4. This is similar to the apical dominance of trees in a forest with the fixed sunlight by interspecific competitive growth.

Figure 5 shows the SEM images of as-grown and annealed thin films, respectively, prepared for a deposition time of 25 min. No noticeable change in thin film morphology was observed by the annealing process. The XRD patterns of as-grown and annealed tungsten oxide thin films are also shown in Figure 6. The characteristic peaks indicate that WO_x thin films were converted to monoclinic WO_3 thin films from WO_x by annealing. The inset photographs display the colors of the corresponding thin films, which are blue for WO_x thin film before annealing (Figure 6a) and yellow for WO_3 thin film after annealing (Figure 6b).

PEC performance of thin films

The PEC performance of WO_3 photoanodes were evaluated by measuring the IPCE plot and current density-voltage (I–V) curve. Figure 7 presents the IPCE plots of tungsten oxide thin films prepared for different deposition times from 10 to 40 min, which were measured in a 0.5 M H_2SO_4 solution at applied potential of 1.0 V under front illumination. It indicates that the IPCE changes significantly by changing the WO_3 thin film thickness. As the thin film thickness increases from 1.8 μm (10 min deposition) to 7.2 μm (30 min deposition), the IPCE plot shifts up gradually for the whole range of wavelengths from 350 to 500 nm. The maximum IPCE values for

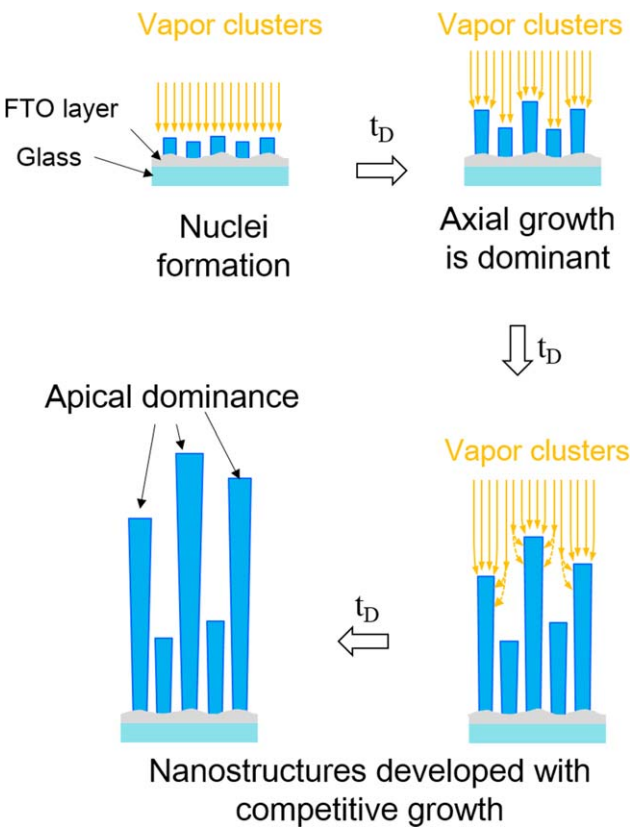

Figure 4. The schematic illustration of nanowire-based structure growth mechanisms.

[Color figure can be viewed in the online issue, which is available at wileyonlinelibrary.com.]

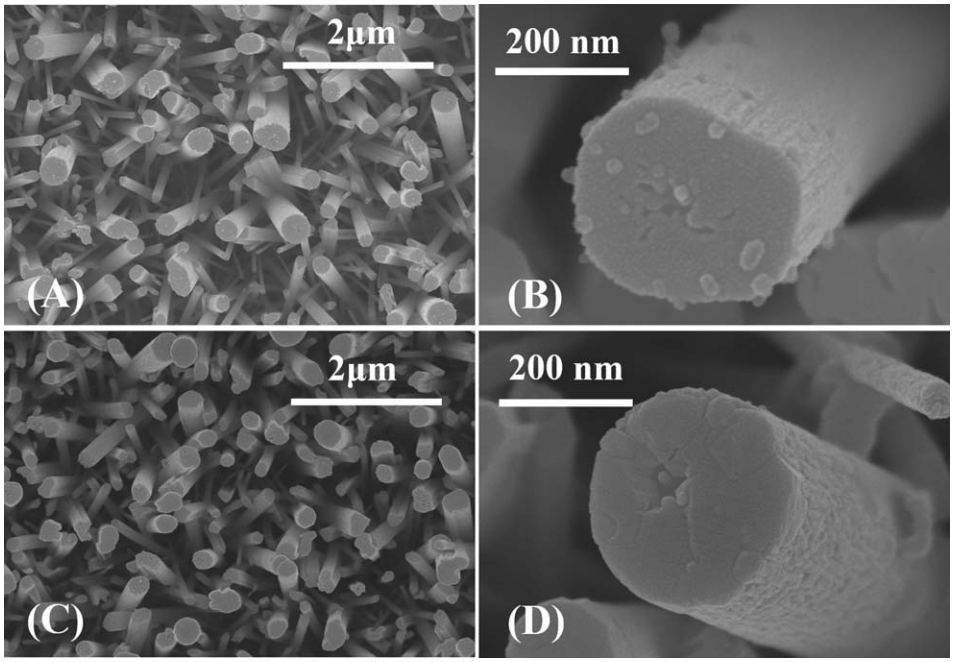

Figure 5. Top view SEM images of as-grown (A, B) and annealed (C, D) tungsten oxide nanostructures prepared for 25 min.

deposition times of 10, 20, 25, and 30 min were 24.0% at 380 nm, 30.2% at 390 nm, 43.6% at 410 nm, and 45.8% at 410 nm, respectively. With increased thin film thickness, more illuminated light could be absorbed to generate more photoelectrons and holes and, thus, a higher photocurrent could be generated. Meanwhile, the peak value of each IPCE plot shifted toward the visible long-wavelength light region from 380 to 410 nm, which implies that more light in the visible region could be utilized for photoexcitation as the thickness increases. This is most probably because the shorter wavelength light which has higher energy could be more efficiently utilized in the thinner thickness of thin film, while the longer wavelength light could be transmitted farther into the thin film with thicker thickness for higher transmittance. As the thickness increased, more light with longer wavelength could efficiently be absorbed for the increased penetration length in thicker thin film. When the thickness increases further, however, the IPCE plot shifts down and the maximum IPCE value decreases to 41.1% for 35 min deposition and 32.2% for 40 min deposition at the same wavelength of 410 nm. When the thin film thickness is beyond the critical value of approximately 7.2 μm, the light absorption of thin film becomes saturated. It is suggested that atomic and structural properties of WO_3 nanowires are constant in our experimental conditions. Electron/hole transport is mainly affected by the length and diameter of WO_3 nanowires as well as the interfacial contact area between nanowire and electrolyte. Further increase in thickness leads to larger interfacial contact area promoting a

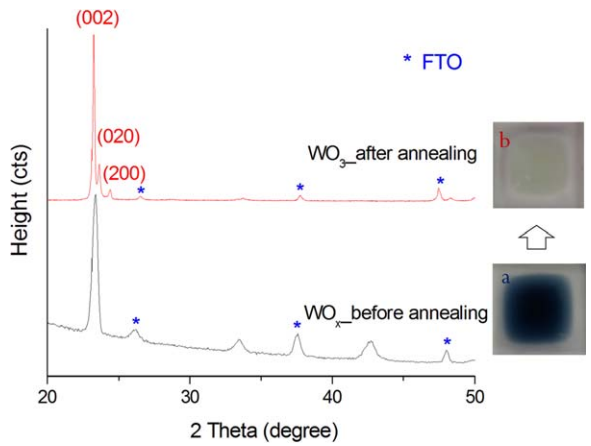

Figure 6. XRD pattern and photographs of as-grown (a) and annealed (b) tungsten oxide thin films prepared for 25 min.

[Color figure can be viewed in the online issue, which is available at wileyonlinelibrary.com.]

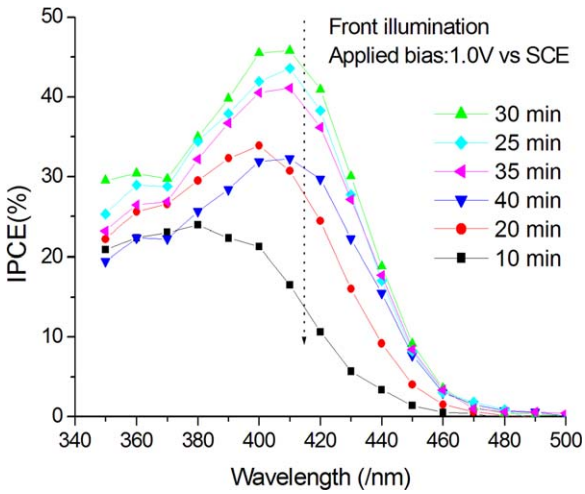

Figure 7. IPCE plots of tungsten oxide thin films prepared for different deposition time measured in 0.5 M H_2SO_4 solution under front illumination at an applied bias of 1.0 V vs. SCE.

[Color figure can be viewed in the online issue, which is available at wileyonlinelibrary.com.]

faster water oxidation reaction. However, as thickness increases, the length and diameter of the WO_3 nanowires increase. The increase in length of the nanowires causes a longer distance or time for the photogenerated electrons to migrate from nanowire-structures to the current collector (FTO) and a longer distance for holes to diffuse to the WO_3/electrolyte interface. Thus, the electrical transport resistances of charge carriers increase. The nanowire-based thin film with longer length and bigger diameter also makes the charge recombination processes more competitive with the transport of photoelectrons and holes promoting the electron-hole recombination and reduction in the IPCE result.[19] Thus, light absorption and charge transport has to be balanced to maximize efficiency. The best-performing photoanode consisting of WO_3 nanowire-structures with an average length (thin film thickness) of 7.2 μm and average diameter of 260 nm at the tip of nanowire-based structures were prepared for 30 min deposition. The average length for best performance here is comparable with the value (6.0 μm) proposed in the literature[11] for dense WO_3 film to reach saturation of light absorption. The average diameter of nanowire-based structures for best performance is also close to 300 nm (double of the reported hole diffusion length in the literature[11]) leading to efficient hole injection. It indicates that this nanowire-based thin film with optimal length and diameter could counterbalance the light absorption yield and charges transport losses and, thus, maximize the IPCE results.

Figure 8A shows the IPCE plots of as-grown WO_x under front illumination and annealed WO_3 photoanode under front and back illumination. All photoanodes measured for Figure 8 were assembled with the thin films prepared for 30 minutes deposition. IPCE for as-grown WO_x thin film is extremely low compared to that for annealed WO_3 thin film, because the substoichiometric WO_x has many oxygen vacancies which work as recombination sites, where photogenerated electron-hole pairs would be recombined, leading to reduced efficiency. It is proven that WO_x is non-photoactive and all as-grown thin films should be converted to photoactive WO_3 for further PEC water splitting application. The PEC performance of annealed thin film under back illumination was also examined in this study and Figure 8A shows that thin film exhibits the higher IPCE under front illumination than that obtained under back illumination. With back illumination, the WO_3 thin film-coated side is facing toward the CE and would facilitate the proton generated to travel shorter distance to the CE, which promotes water oxidation ($2H_2O(l) + 4h^+ \rightarrow 4H^+ + O_2(g)$) at the WO_3/electrolyte interface. However, as the incident light has to pass through FTO-coated glass (2 mm thick) to reach WO_3 thin film, some light would be partially adsorbed, reflected and lost in the FTO-coated glass. When the WO_3 thin film-coated side faces toward the light source under front illumination, light can be harvested by WO_3 thin film more efficiently than that under back illumination, but protons generated travel longer distances to the CE. It implies that the impact of light absorption by FTO-coated glass is far larger than that of the proton transport on PEC performance for back illumination. Figure 8B shows the IPCE plots with thin films prepared for 30 minutes deposition with respect to various applied potentials between WE and CE electrodes. The IPCE plot presents the similar tendency for all cases and it shifts up with increasing the applied potential. The higher the applied potential is, the more effective the electron-hole separation is and, thus, the faster transport and collection of photogenerated

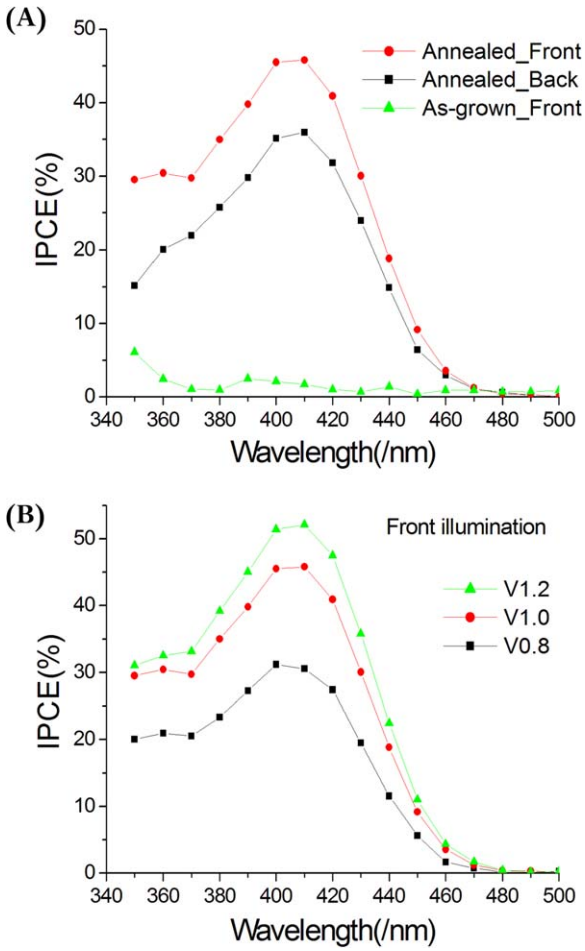

Figure 8. (A) IPCE plots for as-grown (WO_x) and annealed (WO_3) thin films measured under front illumination, and for annealed thin film measured under back illumination, respectively (at an applied potential of 1.0 V vs. SCE); (B) IPCE plots for WO_3 thin films with various applied potentials under front illumination.

All thin films for A and B were prepared for 30 min deposition and measured in 0.5 M H_2SO_4 solution. [Color figure can be viewed in the online issue, which is available at wileyonlinelibrary.com.]

charges could be achieved, resulting in the higher IPCE results.

Linear scan voltammetry was performed to obtain the I–V curves in 0.5 M H_2SO_4 solution as shown in Figure 9 with thin films prepared for various deposition times under dark conditions and under front illumination of simulated AM1.5 solar light (100 m W cm^{-2}), respectively. Under dark conditions, current density is close to zero for all cases. When the light is on, the onset photocurrent begins at around 0.3 V vs. SCE. It is worth mentioning that the small current observed below 0.3 V for both dark and light illuminated conditions is ascribed to the electrochromic redox response of H_xWO_3/WO_3 ($H_xWO_3 \rightarrow WO_3 + xH^+ + xe^-$).[20] Above 0.3 V, the photocurrent increases with the increase of applied bias voltage for all cases due to the enhanced charge separation at more positive potential. Current density increases quickly as the applied potential increases from 0.3 to about 1.0 V but, later, increases relatively slowly as the applied potential increases from 1.0 to about 1.8 V. Eventually it will reach saturation as the applied

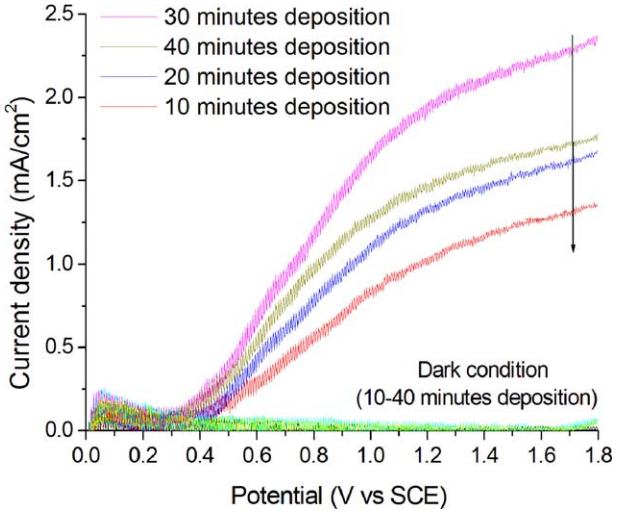

Figure 9. I–V curves of tungsten oxide thin films with respect to different deposition times measured in dark and under front illumination of simulated AM1.5 solar light (100 mW cm^{-2}) in 0.5 M H_2SO_4 solution.

[Color figure can be viewed in the online issue, which is available at wileyonlinelibrary.com.]

potential increases further and the maximum solar current density will depend on the semiconductor material. Still, the thin film prepared for 30 min deposition exhibits the highest current density compared to other thicknesses for all applied potentials. This is consistent with the trend indicated in IPCE plots (Figure 7). Photocurrent density increases with the increase of thin film thickness below the critical value, light absorption is the determinant factor. And beyond this critical value where light absorption is saturated and charge separation and transport in long-range distance becomes the limiting factor, photocurrent density decreases with the increase of thin film thickness. Thus, photocurrent density of thin film prepared for 40 min is lower for the entire range of applied potential than that for 30 min.

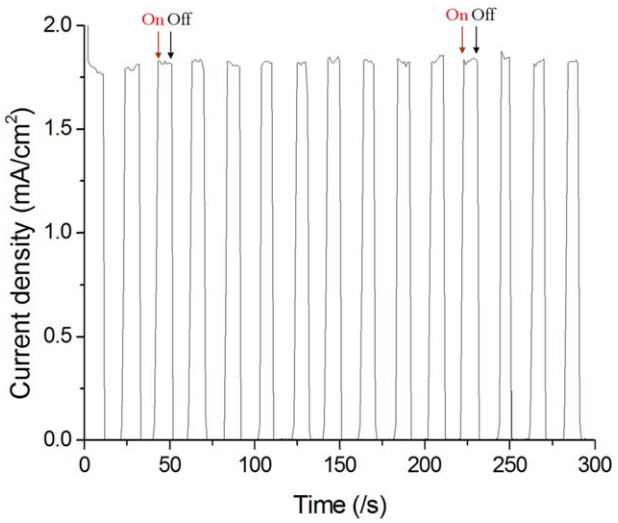

Figure 10. The photocurrent density-time (*J-t*) curves of WO_3 deposited for 30 min, measured under a chopped illumination of AM1.5 G at an interval of 10 s on/off for at an applied potential of 1.0 V vs. SCE.

[Color figure can be viewed in the online issue, which is available at wileyonlinelibrary.com.]

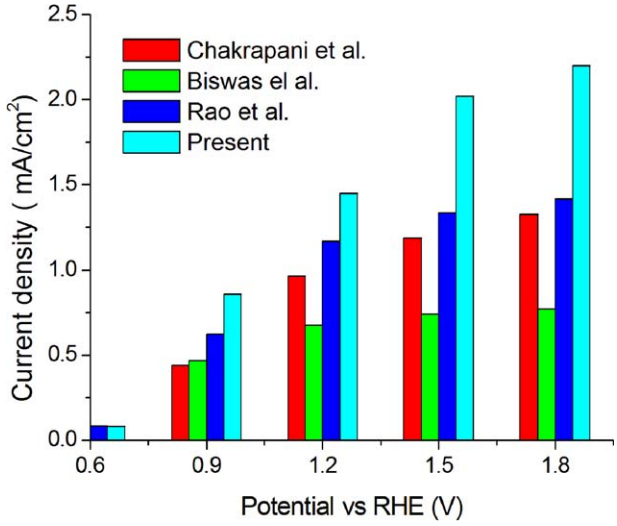

Figure 11. Histogram comparison of the reported photocurrent values in the literature at different applied voltages.

[Color figure can be viewed in the online issue, which is available at wileyonlinelibrary.com.]

The photocurrent density (J)-time (t) scan of thin film prepared for 30 min was performed under a chopped illumination of AM1.5 G with an interval of 10 s on/off at an applied bias of 1.0 V vs. SCE, the result of which is shown in Figure 10. The abrupt occurrence and decay of the photocurrent density during the on/off illumination sequences implies the fast conduction of photogenerated electrons from WO_3 to FTO. The photocurrents in the J-t curves remain nearly constant and match closely with the values in I–V curves at 1.0 V vs. SCE for the same thin film thickness, indicating that the present 1-D nanostructured WO_3 thin films prepared in this study are quite stable over many on/off cycles.

Histogram comparison of the photocurrent values in this study with state-of-the-art nanostructured WO_3 photoanodes taken from the literature at different applied potentials is shown in Figure 11. Chakrapani et al.[12] reported WO_3 nanowires by a CVD process and Biswas et al.[16] prepared nanocrystals by a hydrothermal method and both tested the IPCE in 0.5 M H_2SO_4 solution. Rao et al.[15] prepared nanowires by a FVD method and measured the IPCE in 0.5 M potassium phosphate electrolyte. To make a comparison, the applied potentials reported in the literature are all converted to the values against a reversible hydrogen electrode (RHE) according to Nernst equations[21]: E_{RHE} (V) = $E_{Ag/AgCl}$ + [0.059 (V) *PH] + $E^0_{Ag/AgCl}$ (0.194 V) or E_{RHE} (V) = $E_{SCE/KCl}$ + [0.059 (V) *PH] + $E^0_{SCE/KCl}$ (0.242V), at 25°C. Nanowire-based structures prepared by CVD and FVD processes showed better performance than nanocrystal-based photoanode. The best-performing WO_3 nanowire-based structured photoanode in this study exhibits significantly improved performance over that of flame synthesized nanowire (Rao et al. reported) for all range of applied potentials.

Conclusions

Facile growth of WO_x thin films with desirable thickness based on vertically-aligned nanowire-structures was realized using a FVD process incorporated with a constant tungsten

feeding system. Nonphotoactive WO_x could be converted to photoactive monoclinic WO_3 by postannealing at 450°C for 2 h in atmospheric condition. As deposition time increases, the length and diameter of individual structures of thin film grows larger and larger simultaneously. The feasible growth mechanisms of nanowire-based structure were proposed. Nanowire-based WO_3 thin film with optimum thickness of 7.2 μm was found to have the best performance for PEC water splitting under front illumination. When below this critical value, the increase of thin film thickness enhances light absorption and more photocurrent could be generated. As the thickness increases further beyond the optimum thickness, the photocurrent decreases because of limited charge separation and transport in the long-range structure. The present nanowire-based WO_3 thin film with optimum thickness demonstrated better IPCE performance than those of nanostructured WO_3 photoanodes in previous literature. This work offers a promising approach to prepare the 1-D nanostructured WO_3 thin film with precise thickness control.

Acknowledgments

This research was supported by the Converging Research Center Program through the Ministry of Science, ICT and Future Planning (grant number 2014048827). Instrumental analysis was supported from the central laboratory of Kangwon National University.

Literature Cited

1. Van DK, Liang Y, Schoonman J. Solar hydrogen production with nanostructured metal oxides. *J Mater Chem*. 2008;18:2311–2320.
2. Yin W, Tang H, Wei S, Al-Jassim M, Turner J, Yan Y. Band structure engineering of semiconductors for enhanced photoelectrochemical water splitting: the case of TiO_2. *Phys Rev B*. 2010;82:045106.
3. Holladay JD, Hu J, King DL, Wang Y. An overview of hydrogen production technologies. *Catalysis Today*. 2009;139:244–260.
4. Rauh RD, Buzby JM, Reise TF, Alkaitis SA. Design and evaluation of new oxide photoanodes for the photoelectrolysis of water with solar energy. *J Phys Chem*. 1979;83:2221–2226.
5. Liu Y, Xie S, Liu C, Li J, Lu X, Tong Y. Facile synthesis of tungsten oxide nanostructures for efficient photoelectrochemical water oxidation. *J Power Sources*. 2014;269:98–103.
6. Santato C, Ulmann M, Augustynski J. Photoelectrochemical properties of nanostructured tungsten trioxide films. *J Phys Chem B*. 2001; 105:936–940.
7. Rao PM, Cho IS, Zheng X. Flame synthesis of WO_3 nanotubes and nanowires for efficient photoelectrochemical water-splitting. *Proc Combust Inst*. 2013;34:2187–2195.
8. Su J, Feng X, Sloppy JD, Guo L, Grimes CA. Vertically aligned WO_3 nanowire arrays grown directly on transparent conducting oxide coated glass: synthesis and photoelectrochemical properties. *Nano Lett*. 2011;11:203–208.
9. Kalanur SS, Hwang YJ, Chae SY, Joo OS. Facile growth of aligned WO_3 nanorods on FTO substrate for enhanced photoanodic water oxidation activity. *J Mater Chem A*. 2013;1:3479–3488.
10. Kim H, Senthil K, Yong K. Photoelectrochemical and photocatalytic properties of tungsten oxide nanorods grown by thermal evaporation. *Mater Chem Phys*. 2010;120:452–455.
11. Butler MA. Photoelectrolysis and physical properties of the semiconducting electrode WO_3. *J Appl Phys*. 1977;48:1914–1920.
12. Chakrapani V, Thangala J, Sunkara MK. WO_3 and W_2N nanowire arrays for photoelectrochemical hydrogen production. *Int J Hydrogen Energy*. 2009;34:9050–9059.
13. Rao PM, Zheng X. Unique magnetic properties of single crystal γ-Fe_2O_3 nanowires synthesized by flame vapor deposition. *Nano Lett*. 2011;11:2390–2395.
14. Height MJ, Madler L, Pratsinis SE. Nanorods of ZnO made by flame spray pyrolysis. *Chem Mater*. 2006;18:572–578.
15. Rao PM, Cai L, Liu C, Cho IS, Lee CH, Weisse JM, Yang P, Zheng X. Simultaneously efficient light absorption and charge separation in WO_3/$BiVO_4$ core/shell nanowire photoanode for photoelectrochemical water oxidation. *Nano Lett*. 2014;14:1099–1105.
16. Biswas SK, Baeg J, Moon S, Kong K, So W. Morphologically different WO_3 nanocrystals in photoelectrochemical water oxidation. *J Nanopart Res*. 2012;14:1–12.
17. An W, Thimsen E, Biswas P. Aerosol-chemical vapor deposition method for synthesis of nanostructured metal oxide thin films with controlled morphology. *J Phys Chem Lett*. 2010;1:249–253.
18. Thimsen E, Rastgar N, Biswas P. Nanostructured TiO_2 films with controlled morphology synthesized in a single step process: performance of dye-sensitized solar cells and photo watersplitting. *J Phys Chem C*. 2008;112:4134–4140.
19. Pham H, Kim K. Effect of TiO_2 thin film thickness on NO and SO_2 removals by dielectric barrier discharge-photocatalyst hybrid process. *Ind Eng Chem Res*. 2013;52:5296–5301.
20. Yao Z, Di J, Yong Z, Zhao Z, Li Q. Aligned coaxial tungsten oxide-carbon nanotube sheet: a flexible and gradient electrochromic film. *Chem Commun*. 2012;48:8252–8254.
21. Chae SY, Jung H, Jeon HS, Min BK, Hwang YJ, Joo O. Morphology control of one-dimensional heterojunctions for highly efficient photoanodes used for solar water splitting. *J Mater Chem A*. 2014;2: 11408–11416.

Manuscript received July 6, 2015, and revision received Oct. 20, 2015.